

Supporting Information

Assessing the Optoelectronic Performance of Halide Perovskite Quantum Dots with Identical Bandgaps: Composition Tuning vs. Quantum Confinement

Long Hu^{1,2#}, Xinwei Guan^{3#}, Hehe Huang^{4#}, Tingting Ye⁵, Junfeng Ding⁵, Aarti Aarti⁶, Koushik Venkatesan⁶, Weizhen Wang⁷, Fandi Chen¹, Chun-Ho Lin¹, Tao Wan¹, Mengyao Li, Jiabao Yi³, Rongkun Zheng⁸, Dewei Chu^{1*}, Songhua Cai^{7*}, Jiayi Chen⁹, Claudio Cazorla¹⁰, Jianyu Yuan^{4*}, Yang Bai¹¹, Tom Wu^{1,7*}, Shujuan Huang^{2*}

¹ School of Materials Science and Engineering, University of New South Wales (UNSW), Sydney, NSW, 2052, Australia

² School of Engineering, Macquarie University Sustainable Energy Research Centre, Macquarie University, Sydney, NSW, 2109, Australia

³ Global Innovative Centre for Advanced Nanomaterials, School of Engineering, College of Engineering, Science and Environment, The University of Newcastle, Callaghan, NSW, 2308 Australia

⁴ Institute of Functional Nano & Soft Materials (FUNSOM), Soochow University, Suzhou, Jiangsu 215123, P. R. China

⁵ Key Laboratory of Materials Physics, Institute of Solid-State Physics, Hefei Institutes of Physical Science, Chinese Academy of Sciences, Hefei 230031, China

⁶ School of Natural Sciences, MQ Photonics Research Centre, Macquarie University, Sydney, NSW, 2109, Australia

⁷ Department of Applied Physics, The Hong Kong Polytechnic University, Kowloon, Hong Kong 999077, China

⁸ School of Physics, The University of Sydney, Sydney, NSW 2006, Australia

⁹ School of Molecular and Life Sciences, Curtin University, Bentley, Perth, WA, 6102 Australia

¹⁰ Departament de Física, Universitat Politècnica de Catalunya, Campus Nord B4-B5, E-08034 Barcelona, Spain

¹¹ Faculty of Materials Science and Energy Engineering/Institute of Technology for Carbon Neutrality, Shenzhen Institute of Advanced Technology, Chinese Academy of Sciences, Shenzhen 518055, Guangdong, China

Email: d.chu@unsw.edu.au; songhua.cai@polyu.edu.hk; jyyuan@suda.edu.cn; tom.wu@unsw.edu.au; shujuan.huang@mq.edu.au;

Experimental section: Lead iodide (PbI_2 , 99.999%, Sigma-Aldrich), Lead Bromide (PbBr_2 , 99.999%, Sigma-Aldrich), Cesium carbonate (Cs_2CO_3 , 99%, Sigma-Aldrich), octadecene (ODE, 90%, Sigma-Aldrich), oleic acid (OA, 90%, Sigma-Aldrich), oleylamine (OLA, Sigma-Aldrich, 70%), octane (anhydrous, 95%, Sigma-Aldrich), hexane (anhydrous, $\geq 99\%$, Sigma Aldrich), methyl acetate (MeOAc, anhydrous, 99.5%, Sigma-Aldrich), titanium tetrachloride (TiCl_4 , $\geq 98\%$, Sinopharm Chemical Reagent Co.,Ltd.), chlorobenzene (CB, anhydrous, 99.8%, Sigma-Adlrlich), and PTAA (1-Materials) were used as received without further purification unless mentioned. Glass/FTO was purchased from the Zhuhai Kaivo Optoelectronic Technology Co. Ltd.

CsPbI₃ and CsPbI_{2.5}Br_{0.5} QD synthesis: 0.2 g Cs_2CO_3 was loaded into the mixture of 10 ml ODE and 0.8 ml OA and then this mixture was kept under stirring and vacuum at 120 °C for 1 h to prepare Cs-OA precursor. Two three-neck flasks were used to synthesize CsPbI₃ and CsPbI_{2.5}Br_{0.5} QDs. All conditions were identical except the injection temperature and the ratio of PbI_2 and PbBr_2 for both QD syntheses. For CsPbI₃ QD synthesis, 0.5 g of PbI_2 , 2.5 ml of oleic acid (OA), and 25 ml of octadecene (ODE) were loaded in 100 ml three-neck flask and vacuum pumped under continuous stirring at 100 °C for 1 h. Then, 2.5 ml of oleylamine (OLA) was injected into the flask. After PbI_2 completely dissolved, the temperature was increased to 150 °C under N_2 flow protection. 2 mL Cs-OA precursor was swiftly injected into the reaction mixture, and the solution was quenched by an ice bath. For CsPbI_{2.5}Br_{0.5} QD synthesis, 0.368 g PbI_2 and 0.07 g PbBr_2 were loaded into the mixture of 25 ml ODE and 2.5 ml OA and all other conditions were the same except the injection temperature at 170 °C. Both types of QD solutions were evenly divided into 3 centrifugation tubes and then methyl acetate was added into tubes with the volume ratio of 1:2 (QD solution: methyl acetate). Subsequently, QD precipitate was extracted by centrifugation at the speed of 8000 rpm for 3 min. All QD precipitate in 3 tubes was dispersed with 3 ml hexane and then precipitated by adding 4.5 ml methyl acetate and centrifuged again at 8000 rpm for 3 min. Finally, the extracted QDs were dissolved in octane for further characterization and device fabrication.

Device fabrication and characterizations: Two batches of QD devices were fabricated using the same conditions. The TiO_2 precursor was sprayed onto pre-patterned FTO glass substrates and annealed at 450 °C for 30 min in ambient condition and naturally cooled down to room temperature. The as-synthesized QD octane solution with a concentration of 70 mg/ml was spin-coated on the TiO_2 layer atop of FTO glass at 1000 RPM for 30 s, treated with pure

anhydrous MeOAc for 20 s in the dry box with a relative humidity of 15%. This procedure was repeated 4 times to deposit 350 nm film as an absorber layer. PTAA solution (10 mg/mL in chlorobenzene) was spin-coated on top QD films at 2000 rpm as hole transport layers (HTLs). Finally, 100 nm Au electrodes were prepared by thermal evaporation. The devices were masked with a black metal aperture to define an active area of 0.072 cm².

Material and device characterizations: TEM characterization was carried out using a FEI Tecnai G2 20 microscope. SEM (FEI Nova Nano 630) and AFM (Bruker Dimension ICON) measurements were used to examine the surface morphology of quantum dot film, respectively. The absorbance spectrum was performed using an Evolution 600 ultraviolet–visible spectrophotometer (Thermo Scientific). The pressure-induced PL measurements were conducted in a diamond anvil cell (DAC) with a culet size of a 500 μm diameter. Then, a center hole with a diameter of approximately 170 μm was drilled by focused laser ablation as the sample chamber. A ruby ball with a diameter of approximately 5 μm was loaded into the sample chamber in the DAC to calibrate the pressure. The 532 nm lines of the incident laser were employed as the excitation source for PL. The temperature-dependent steady state and time-resolved PL measurements were carried out using the FLS980 Edinburg Instrument. FTIR was performed through a Thermo Fisher FTIR6700. XPS and UPS measurements were conducted by a VG ESCALAB MK2 system with monochromatized Al K α radiation under a pressure of 5.0×10^{-7} Pa. The transient absorption was carried out under ambient conditions, the fs-TA measurements were performed on a Helios pump-probe system (Ultrafast Systems LLC) combined with an amplified femtosecond laser system. STEM observations of the QD specimens were carried out in an aberration-corrected STEM microscope (Spectra 300, Thermofisher equipped with a field emission gun) with 300 kV electron beam accelerating voltage. The beam current of the electron probe was reduced to 5 pA to minimize the damage during atomic resolution imaging. The probe convergence angle was 24.5 mrad, and the angular range of the HAADF detector was from 79.5 to 200 mrad.

Solar cells were tested on a Newport AAA solar simulator (94023A-U) with xenon lamp at room temperature using Keithley 2400 (I–V) digital source meter. The intensity of the solar simulator was calibrated to 100 mW/cm² AM 1.5 G by a standard silicon cell with a KG-5 filter. J–V scans and operational stability were measured from forward bias to reverse bias step and from reverse bias to forward (–1.4 V \rightarrow 1.4 V, step 0.0125 V, scan rate: 0.1 V/s) in N₂ filled glovebox. For the light intensity dependence measurement, neutral density filters were used with optical densities ranging from 0.1 to 1 with 0.2 increments.

Simulation Methods: First-principles calculations based on density functional theory (DFT) were carried out with the PBEsol exchange-correlation energy functional,^{1, 2} as it is implemented in the VASP software.³ The projector-augmented wave method (PAW) was employed to represent the ionic cores by considering the following electronic states as valence: Cs 5s 5p 6s; Pb 6p 5d 6s; I 6s 5p; Br 5s 4p.⁴ The Grimme's D3 scheme was employed for a better treatment of the dispersion interactions in the system.⁵ An energy cutoff of 750 eV and a dense Monkhorst-Pack k-point density (equal to that of a 14×14×14 grid for a 5-atom bulk cubic unit cell) were used for integrations within the Brillouin zone, leading to total energies converged to within 1 meV per atom. Atomic relaxations were concluded when the forces in the atoms were all below 0.005 eV/Å. The electronic properties of the the different quantum dots were estimated with the accurate screened hybrid exchange-correlation functional HSE06,⁶ considering the geometries previously relaxed at the PBEsol+D3 level. The cells employed for the simulation of quantum dots, including an ample vacuum region, were as large as 60 Å x 60 Å x 60 Å. The smallest simulated QD contained a total of 15 atoms while the largest 429 atoms. The pressure dependence of the energy band gap of halide QD was assumed to be equivalent to that of the analogous bulk systems. The pressure dependence of the energy band gap of bulk halide perovskites was estimated by performing DFT calculations at several different volumes. Halide vacancy formation energy calculations were performed in supercells containing eight formula units and considering different crystallographic inequivalent positions for the location of the point defects.

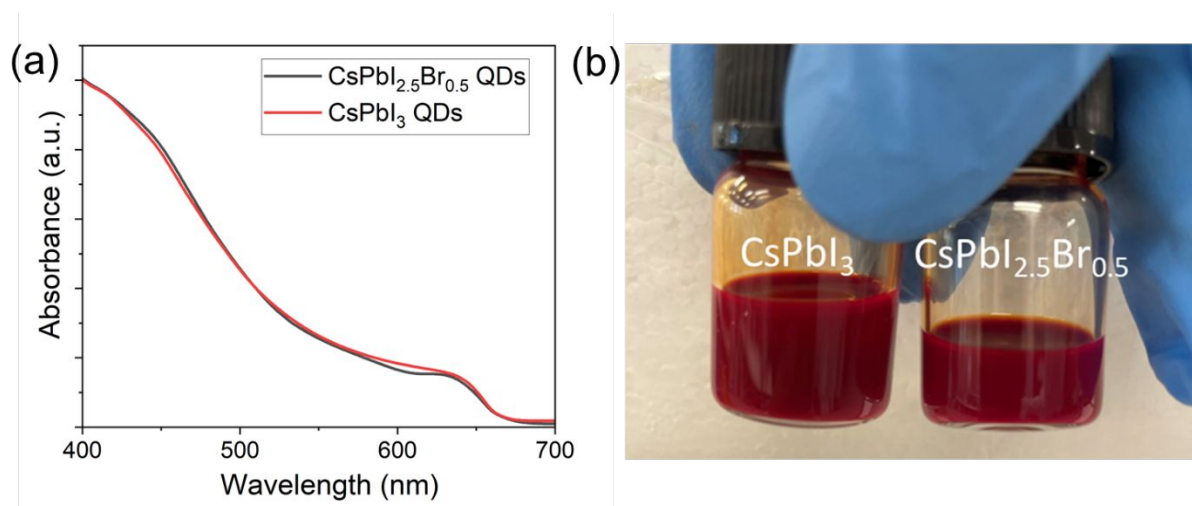


Figure S1. (a) Ultraviolet-visible absorption spectra of both QD solutions. (b) Photography of QD solutions.

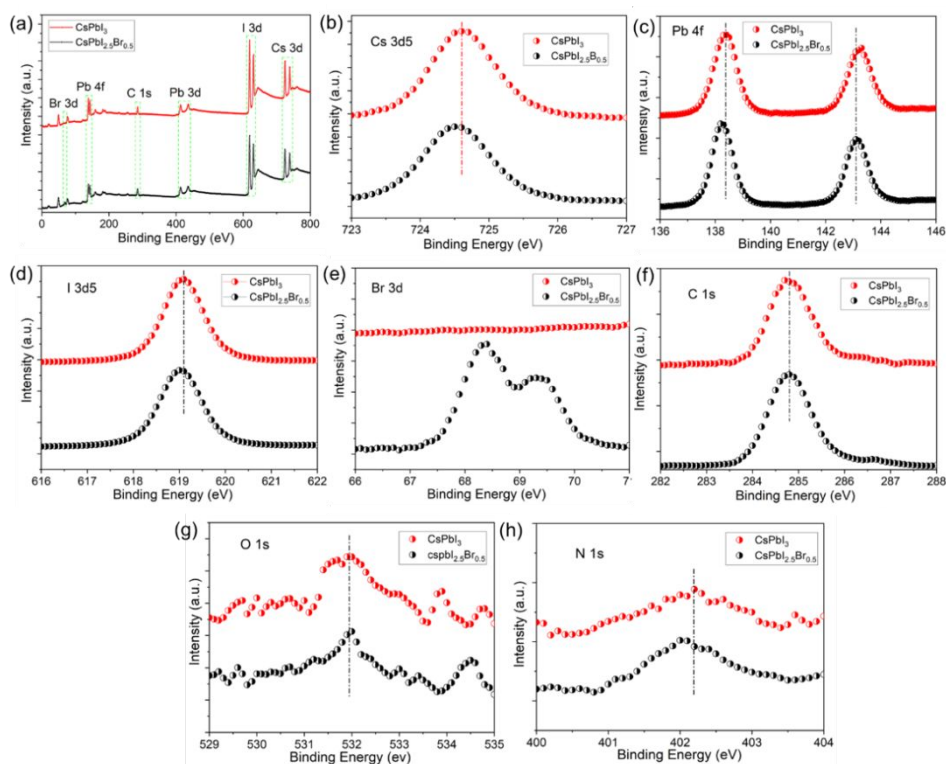


Figure S2. (a) Full XPS spectra and elemental core spectra of (b) Cs 3d₅, (c) Pb 4f, (d) I 3d₅, (e) Br 3d, (f) C 1s, (g) O 1s, and (h) N 1s for both QD films.

Table S1. The elemental percentages of CsPbI₃ QDs and CsPbI_{2.5}Br_{0.5} QDs.

Atomic (%)	Cs	Pb	I	Br	N	O	C
CsPbI ₃	8.4	9.6	24.0	0.0	1.75	4.2	52.0
CsPbI _{2.5} Br _{0.5}	8.6	9.5	19.4	3.8	1.6	4.4	51.1

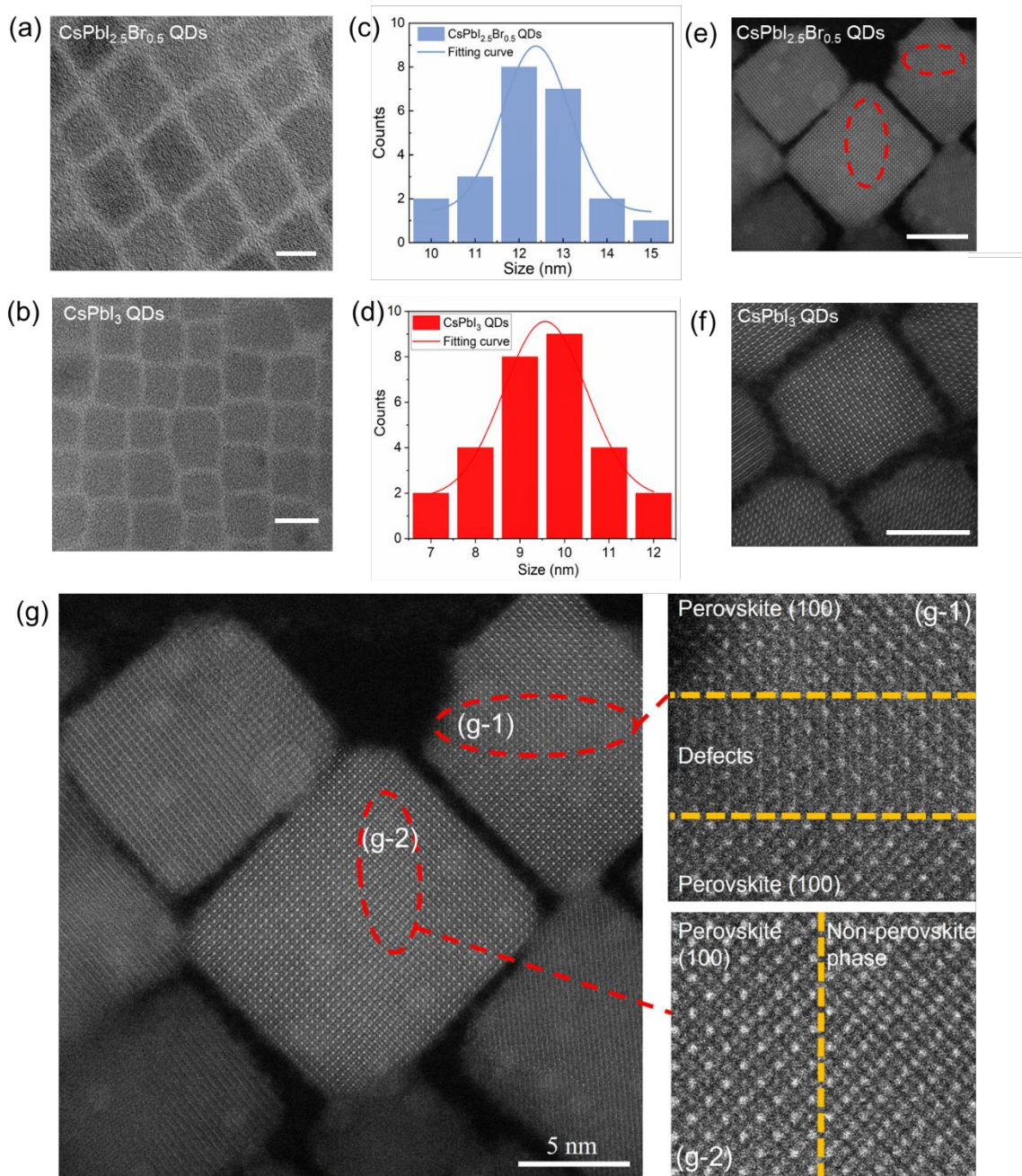


Figure S3. TEM images of (a) CsPbI_{2.5}Br_{0.5} QDs and (b) CsPbI₃ QDs, Size distribution (c) CsPbI_{2.5}Br_{0.5} QDs and (d) CsPbI₃ QDs (Scale bar: 10 nm), STEM images (e) CsPbI_{2.5}Br_{0.5} QDs and (f) CsPbI₃ QDs (Scale bar: 5 nm), (g) magnified lattice structures with (g-1) defect area and (g-2) non-perovskite phase in 001 plane of CsPbI_{2.5}Br_{0.5} QDs.

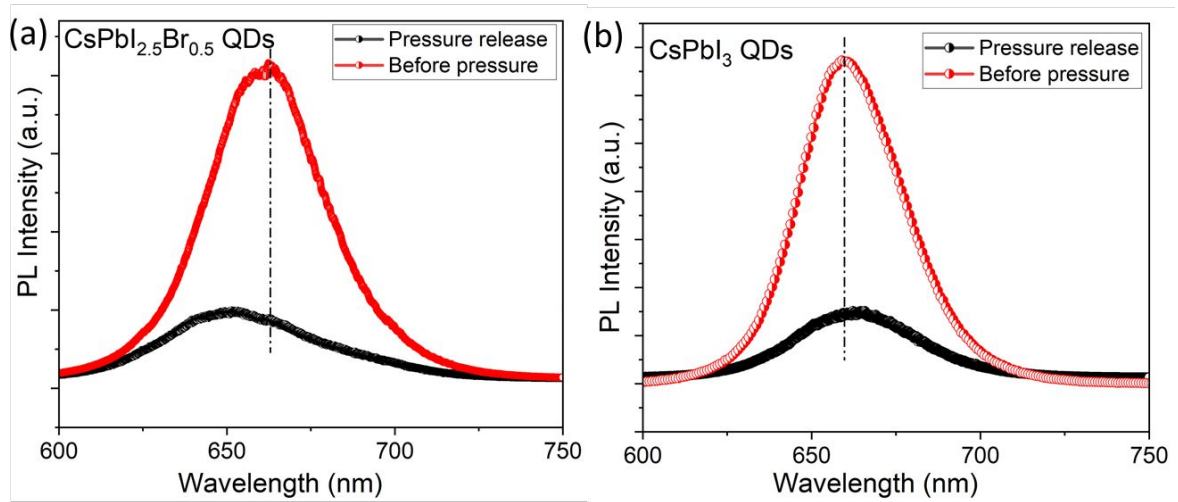


Figure S4. PL characteristics of (a) CsPbI_{2.5}Br_{0.5} QDs and (b) CsPbI₃ QDs before applying pressure and after pressure release.

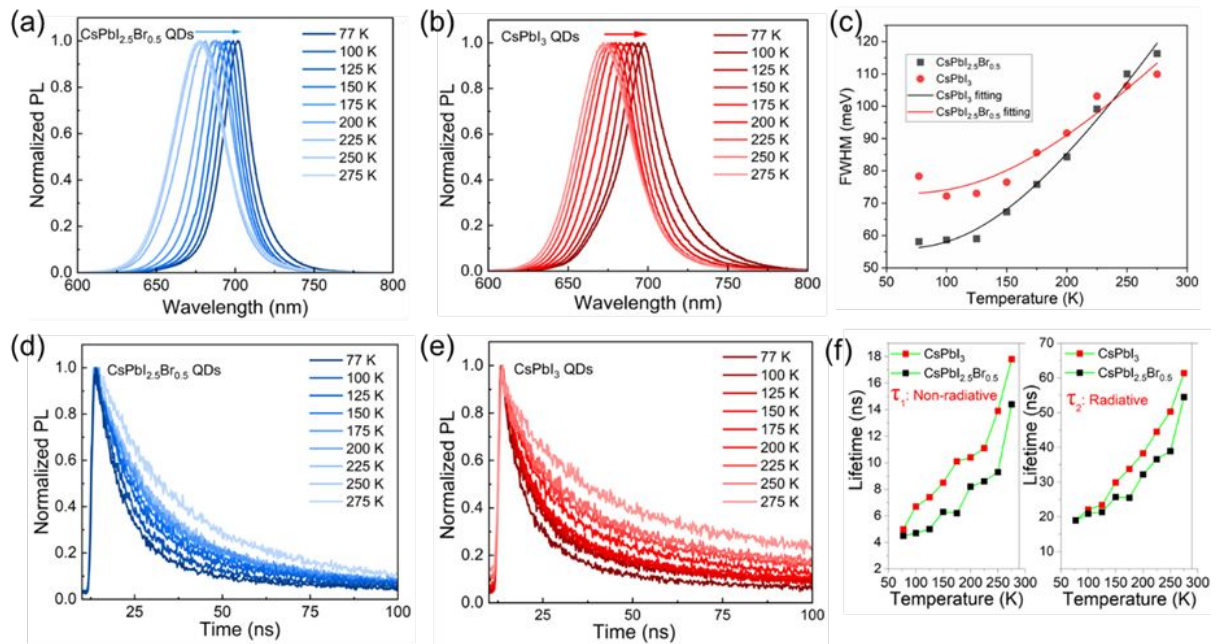


Figure S5. Normalized steady-state PL behaviors of (a) CsPbI_{2.5}Br_{0.5} QDs and (b) CsPbI₃ QDs under different temperatures. (c) FWHM as a function of temperature for both types of QDs. Normalized TRPL decay curves of (d) CsPbI_{2.5}Br_{0.5} QDs and (e) CsPbI₃ QDs. (f) Lifetimes τ_1 and τ_2 of these two types of QDs as functions of temperature.

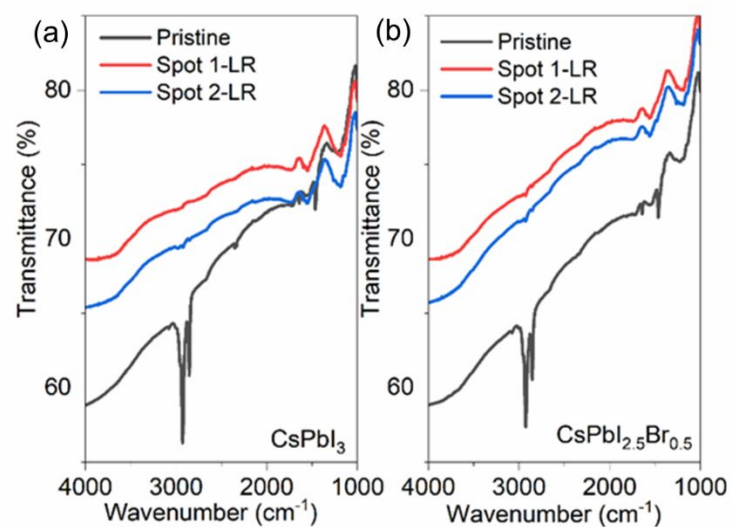


Figure S6. FTIR spectra of (a) CsPbI_3 QD film (b) $\text{CsPbI}_{2.5}\text{Br}_{0.5}$ QD film collected on the two spots after ligand removals.

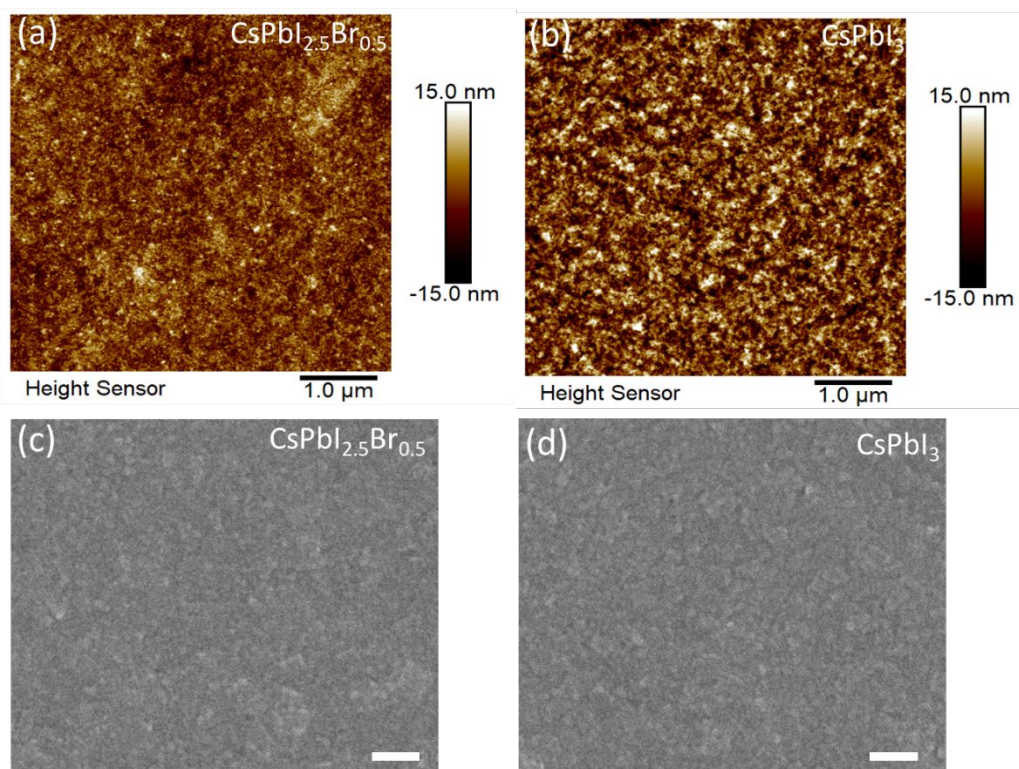


Figure S7. AFM images of (a) $\text{CsPbI}_{2.5}\text{Br}_{0.5}$ and (b) CsPbI_3 QD films. SEM images of $\text{CsPbI}_{2.5}\text{Br}_{0.5}$ QD and (b) CsPbI_3 QD films (Scale bar: 500 nm).

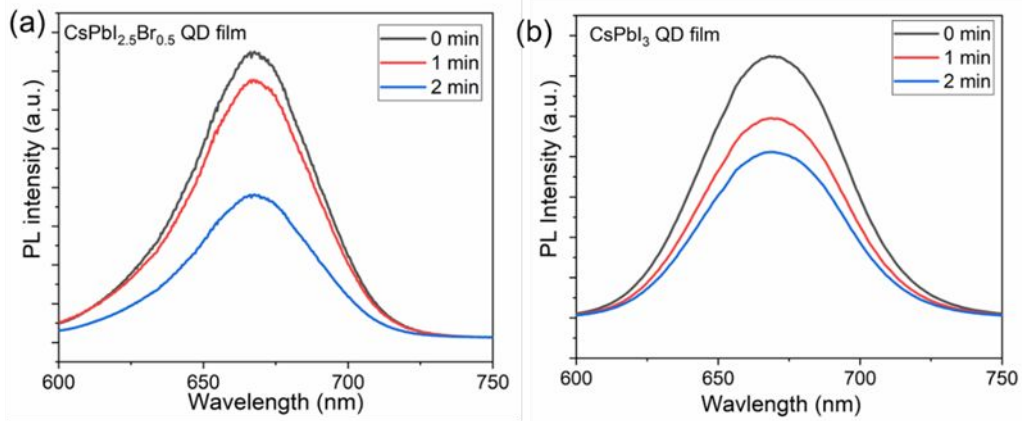


Figure S8. Steady state PL spectra under continuous light illumination (a) CsPbI_{2.5}Br_{0.5} QD film (b) CsPbI₃ QD film with bandgaps of 1.85 eV.

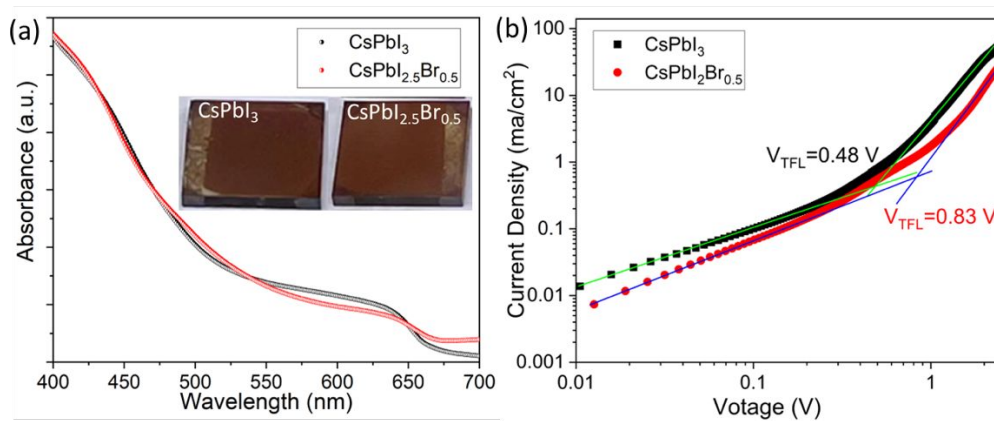


Figure S9. (a) Light absorption curves of CsPbI_{2.5}Br_{0.5} QD and CsPbI₃ QD films (inset image: optical photographs of both QD films). (b) SCLC curves of CsPbI_{2.5}Br_{0.5} QD and CsPbI₃ QD films.

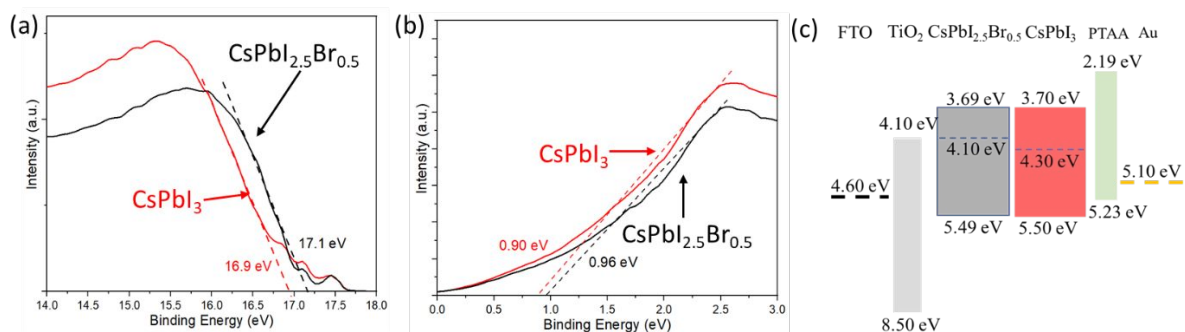


Figure S10. (a) UPS spectra of (a) the cutoff and (b) valence band edge regions of both QD films. (c) Energy-level diagram of both QD solar cells.

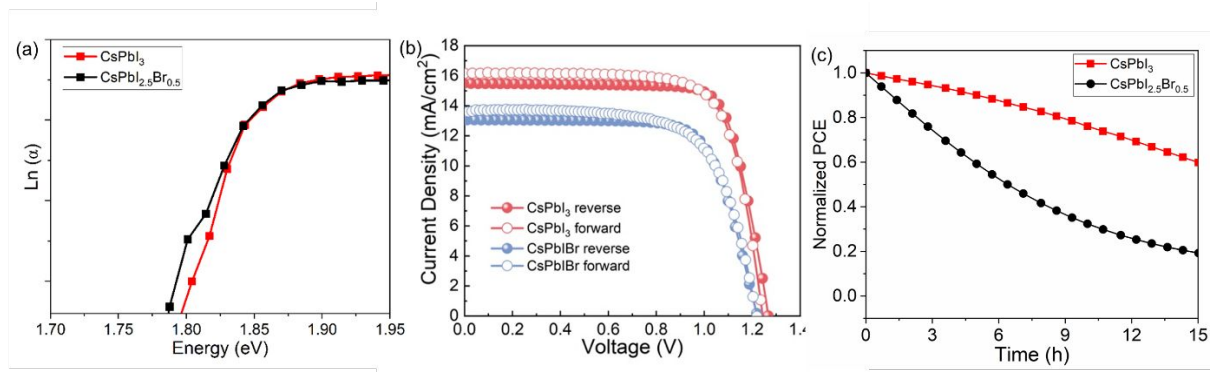


Figure S11. (a) The semi-logarithmic plot to extract the Urbach energy of both QD cells. (b) J-V curves measured from forward and reverse scans in both QD solar cells. (c) Operational stability of both QD solar cells.

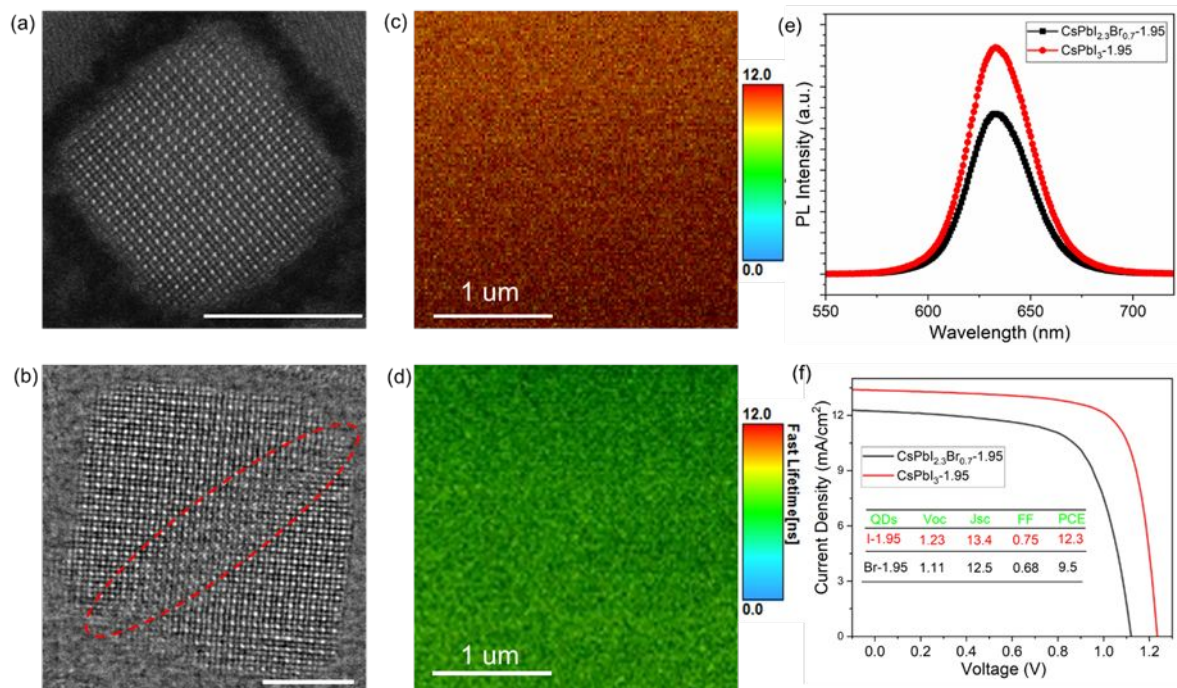


Figure S12. STEM images (a) 1.95-CsPbI₃ QD film (b) 1.95-CsPbI_{2.3}Br_{0.7} QD film (scale bar: 5 nm). Carrier lifetime mapping (c) 1.95-CsPbI₃ QD film (d) 1.95-CsPbI_{2.3}Br_{0.7} QD film. (e) Steady state PL spectra of both types of 1.95 eV QDs. (f) J-V characteristics of both types of 1.95 eV QD champion solar cells.

Reference

- (1) Cazorla, C.; Boronat, J. Simulation and understanding of atomic and molecular quantum crystals. *Rev. Mod. Phys.* **2017**, *89* (3), 035003. DOI: 10.1103/RevModPhys.89.035003.
- (2) Perdew, J. P.; Ruzsinszky, A.; Csonka, G. I.; Vydrov, O. A.; Scuseria, G. E.; Constantin, L. A.; Zhou, X.; Burke, K. Restoring the density-gradient expansion for exchange in solids and surfaces. *Phys. Rev. Lett.* **2008**, *100* (13), 136406. DOI: 10.1103/PhysRevLett.100.136406.

- (3) Kresse, G.; Furthmuller, J. Efficient iterative schemes for ab initio total-energy calculations using a plane-wave basis set. *Phys. Rev. B Condens. Matter* **1996**, *54* (16), 11169-11186. DOI: 10.1103/physrevb.54.11169.
- (4) Blochl, P. E. Projector augmented-wave method. *Phys. Rev. B Condens. Matter* **1994**, *50* (24), 17953-17979. DOI: 10.1103/physrevb.50.17953.
- (5) Grimme, S.; Antony, J.; Ehrlich, S.; Krieg, H. A consistent and accurate ab initio parametrization of density functional dispersion correction (DFT-D) for the 94 elements H-Pu. *J. Chem. Phys.* **2010**, *132* (15), 154104. DOI: 10.1063/1.3382344.
- (6) Brothers, E. N.; Izmaylov, A. F.; Normand, J. O.; Barone, V.; Scuseria, G. E. Accurate solid-state band gaps via screened hybrid electronic structure calculations. *J. Chem. Phys.* **2008**, *129* (1), 011102. DOI: 10.1063/1.2955460.